Electronic Supplementary Material (ESI) for Nanoscale Advances.
This journal is © The Royal Society of Chemistry 2024

SUPPORTING INFORMATION

Dynamic Macromolecular Material Design: The Versatility of Cucurbituril over Cyclodextrin in Host-Guest Chemistry

Jinnipha Pajoubpong,[a] Collin M. Mayhan,[‡a,b] Ajaz Ahmad Dar,[‡a] Alexander I. Greenwood,[c] Karoline C. Klebba,[b] Matthew L. Cremer,[b] and Harshita Kumari[a]*

Table of Contents

Experimental Procedures

Materials

AVO (purity >98.0%, MW 310.39) was purchased from TCI Chemicals. β-CD (purity 98%, MW 1135) was purchased from Acros Organics. CB[7] for NMR, FTIR analyses was synthesized using the method provided in the Supporting Information. CB[7] for UV-Vis analysis was purchased from Boc Sciences (purity >95.0%, MW 1163). Deionized water was obtained from a Milli-Q purification system (Millipore). HPLC-grade ethanol was used. DMSO-d_6 for NMR analysis was purchased from Cambridge Isotope Laboratories.

Instrumentation

^{1}H-NMR spectroscopy

^{1}H NMR spectra were acquired using a Bruker AV-400 (400 MHz) spectrometer. DMSO-d_6, Ethanol-d_6 was utilized as the solvent. Chemical shifts are reported in ppm and calibrated against the DMSO-d_6 peak at 2.5000 ppm as an internal reference.

NOESY and DOSY analysis

The stock solutions of AVO in ethanol-d_1/ethanol-d_6 (10 mM), CB[7] in D_2O (5 mM), and β-CD in D_2O (10 mM) were combined to create mixtures with a fixed AVO concentration at 0.5 mM. For AVO+CB[7], these mixtures included CB[7] at concentrations of 0.5, 1.5, and 3 mM, resulting in molar ratios of 1:1, 1:3 and 1:6. Additionally, for AVO+ β-CD, the mixture included β-CD at a concentration of 5 mM, resulting in a molar ratio of 1:10.The solvent composition for all samples was 90% D_2O and 10% ethanol-d_1/ethanol-d_6.

FTIR spectroscopy

FTIR spectra were collected using a Nicolet 6700 FTIR spectrophotometer equipped with a Smart Orbit diamond ATR module. The spectra were recorded in the range of 4000–400 cm^{-1}.

UV-Vis spectroscopy

UV spectra were collected using a BioTek Epoch 2 microplate spectrophotometer with a quartz cuvette (1 mL, 10 mm path). The spectral range was 220–450 nm with a step size of 5 nm.

HPLC-UV analysis

The HPLC analysis was conducted using a Shimadzu apparatus equipped with a Model LC-20AT pump, a Model SIL-20A injection valve featuring a 50 µL sample loop, and a Model SPD-20A UV-Vis-detector. An Agilent Microsorb-MV 100-5 C18 column (5 µm pore size, 150 × 4.6 mm), operating at room temperature under isocratic conditions, was employed as the analytical column. The mobile phase consisted of methanol/acetonitrile/water/acetic acid (65:20:14.5:0.5, v/v) at a flow rate of 0.8 mL/min. Detection was carried out at 360 nm, and the retention time was approximately 8.5 min. The chromatographic peaks were integrated using the LCSolutions software.

ESI-MS analysis

Mass spectra were acquired using a timsTOF Pro mass spectrometer (Bruker Daltonics). AVO–CB[7] and AVO–β-CD solutions were prepared in a 50:50 (v/v) mixture of water/acetonitrile containing 0.1% formic acid. This solvent was chosen as optimal following a comparison of methanol/water and acetonitrile/water mixtures. A small quantity of each sample was collected using a pipet tip and then dissolved in 200 mL of the solvent. Each sample was then infused directly into the mass spectrometer using a syringe pump at a flow rate of 5 mL/min, and data was acquired for 1 min in the positive ion mode. The raw data were subsequently analyzed using the Bruker Compass DataAnalysis software.

Synthesis of CB[7]

Glycoluril (50 g) and paraformaldehyde (Acros Organic) (21.2 g) were mixed and then reacted in the presence of cold HCl (350 mL, 6 M). The mixture was then heated at 85 °C for 5 days. The crude CB[7] was precipitated out by adding methanol (80% (v/v) of total solution volume) into the mother liquid. The precipitate was collected, washed using methanol, and dried in an oven at a low temperature for 12 hrs. Afterwards, the dried crude CB[7] was dissolved in water (150 mL per 6 g of dried crude). The water-soluble part was collected by filtration. HCl (10% (v/v) of the total volume) was added to the filtrate to crystallize out impurities. After filtration, methanol (80% (v/v) of total solution volume) was added to the filtrate and the second precipitate (mainly CB[7]) was collected, washed using methanol, and dried in an oven at a low temperature for 12 hrs.

Preparation of AVO–β-CD and AVO–CB[7] complexes

Kneading method

The AVO–CB[7] complexes were obtained by grinding AVO with CB[7] at room temperature (22 ± 1 °C) using an agate mortar and pestle. Each compound was weighed at various mole ratios (AVO/CB[7] of 1:0.1 to 1:3), maintaining a constant total mass of 50 mg. The dried mixture was ground in small quantities of water (~100 µL each, 3–4 times) to achieve a white homogenous paste. After continuous grinding for 30 min, additional water was added to create a slurry (2–3 mL), which was then transferred to a 20 mL vial. Subsequently, the dried powder of the AVO–CB[7] complex was obtained by freeze-drying.

Solvent evaporation method

Stock solutions of AVO and β-CD were prepared in ethanol and water, respectively. Aliquots of the AVO and β-CD solutions were mixed to prepare hydro-alcoholic solutions at room temperature (22 ± 1 °C), maintaining a constant ethanol/water ratio of 30:70 (v/v). The AVO/β-CD molar ratio was 1:0.1, 1:0.5, 1:1, or 1:10. Subsequently, the solvent was removed using rotatory evaporation at 45 ± 5 °C to obtain the dried powder of the AVO–β-CD complex.

Determination of stoichiometric ratio and association constant (K_a) by UV-Vis method

Stock solutions of AVO in ethanol (0.8 mM), β-CD in water (10 and 15 mM), and CB[7] in water (4 mM) were combined to prepare solutions with varying β-CD/CB[7] concentrations. The AVO concentration was maintained at 0.04 mM, while the β-CD concentrations ranged from 1 to 7.5 mM and the CB[7] concentrations ranged from 0.2 to 2 mM. The AVO–β-CD and AVO–CB[7] solutions were prepared using ethanol/water ratios of 10:90, 20:80, 30:70, or 40:60 (v/v). The absorbance spectra of AVO in the absence and presence of β-CD/CB[7] were measured. All samples were equilibrated for 30 min prior to measurements. All experiments were conducted in triplicate.

The association constant was calculated using the Benesi–Hildebrand equation, expressed as:

$$\frac{[G]_0}{(A - A_0)} = \frac{1}{K_a \varepsilon [H]} + \frac{1}{\varepsilon} \quad \text{(S1)}$$

where A_0 is the absorbance of AVO in the absence of β-CD/CB[7] at 270 nm, A is the absorbance of AVO in the presence of β-CD/CB[7] at 270 nm, $[G]_0$ is the concentration of AVO, and $[H]$ is the concentration of the host (β-CD or CB[7]). The plots of $[G]_0/(A - A_0)$ versus $1/[H]$ exhibited a linear relationship, indicative of complexes with a 1:1 stoichiometry. The association constant (K_a) was determined by dividing the intercept by the slope. Notably, due to inconsistencies in the absorbance at λ_{max} = 360 nm for the AVO–β-CD complex solutions, the absorbance at 270 nm was used for all calculations.

Computational methods

Molecular dynamics (MD) simulations

All MD simulations were carried out using the AmberTools21 and 23 suite of programs[1]. The GAFF2[2] force field was used for parameters for AVO, CB[7], and β-CD. To obtain better starting structures, the isolated molecules were optimized with the PM6 semi-empirical method. Antechamber[3] with the AM1-BCC method was then used to generate partial charges for these structures. The AVO–CB[7] and AVO–β-CD systems were constructed with AVO in four general configurations relative to β-CD or CB[7]: (1) above (~10 Å) unique openings, (2) at the top rim of unique openings, (3) to the side, and (4) with the t-butyl group (tBu) or methoxy group (MeO) of AVO within the cavity. All of these systems, except AVO above the host, were minimized. The AVO above the host system was not minimized because AVO moved closer to the cavity, resulting in a redundant configuration (see the results and discussion for further details). The systems were solvated with truncated octahedron shells of 10.0 and 15.0 Å comprising of TIP3P H_2O molecules [4]. These solvated systems were then minimized, first with only the solvent molecules and then with all the solute and solvent molecules.

Next, a constant volume simulation with a temperature bath was carried out as the temperature of the system was increased from 0 to 298.15 K over 60 ps with a time step of 0.001 ps; the structures were checked every 10 ps to confirm reasonable structures and system behavior for the heating time. System equilibration continued with NVT and NPT simulations for 30 ps and 500 ps, respectively, with time steps of 0.001 ps. After this equilibration, the host–guest orientation was investigated, and the density of H_2O was compared to the bulk solvent value. The Langevin thermostat[5] with a collision frequency of 3.0 ps^{-1} was used for the NVT and NPT simulations, and the SHAKE algorithm[6] was used to constrain covalent bonds involving hydrogen. The NPT runs implemented a Monte Carlo barostat with isotropic position scaling. These simulations utilized periodic boundary conditions and Ewald's particle mesh method[7] to account for long-range electrostatic interactions, with short-range nonbonded interactions having a cutoff of 0.80

nm. Upon completion of these simulations and identification of the most favorable host–guest interactions, the same starting configurations were used for solutions with different contents of ethanol (10%, 20%, 30%, and 40%, v/v). To construct these systems, the total number of solvent molecules was determined from the simulations in pure H_2O, where 1600 solvent molecules were used for the entrapped AVO orientations, and 3100 solvent molecules were used for AVO above the host. For instance, to model the 10% ethanol solution, 53 ethanol molecules and 1547 water molecules were used; this was determined by using the density of each solvent at 298 K and calculating the molecular ratio. The solvent molecules were monitored throughout the heating process and initial NVT and NPT equilibrations to ensure a homogeneous mixture was obtained.

NPT production runs of 10 ns with a time step of 0.001 ps were carried out for the AVO–β-CD and AVO–CB[7] systems with *t*-Bu and MeO within the cavity in all the ethanol solutions. Another production run was carried out for the configuration with AVO above the host cavity. All analyses of the runs were performed using CPPTraj[8]. The coordinates for all trajectories were sampled every 0.10 ps and visualized in Chimera[9].

Electronic structure calculations

To better understand the host–guest thermodynamics, the isolated molecules (AVO, β-CD, and CB[7]) and the complexes (AVO–CB[7] and AVO–β-CD) were investigated. The starting geometries for the electronic structure calculations were obtained from the initial minimizations of the isolated host–guest systems for the MD simulations. Thus, the electronic structure calculations focused on the following orientations of AVO relative to the host: (1) MeO of AVO within the cavity, (2) tBu of AVO within the cavity, (3) AVO above the opening, and (4) AVO to the side. We recognize that several conformational orientations of these systems on the potential energy surface that were not probed could be more favorable (e.g., there are a number of dihedral angles within AVO that could lead to additional interactions with the cavity). The results primarily focus on the “entrapped” possibilities, with tBu or MeO of AVO included within the cavity. A full explanation of the calculation protocol and orientations can be found in the Supporting Information. Complete optimization with vibrational frequencies at the B3LYP/6-311G(d,p) level of theory were carried out using the Gaussian16[10] suite of programs, and minima were visualized with GaussView6[11]. Single-point energies (SPEs) were calculated using the ωB97X-D and M06-2X methods and the 6-311+G(d,p) and 6-311G(d,p) basis sets. The AVO–CB[7] and AVO–β-CD complexes were also corrected for basis set superposition error (BSSE) using the counterpoise = 2 keyword. In addition to the gas-phase calculation of SPEs, all systems with water and ethanol included implicit solvent effects using the SMD method[12]. The thermodynamic values for the dissociation reactions were calculated based on Equations 2 and 3:

$$\text{AVO–CB[7]} \rightarrow \text{AVO} + \text{CB[7]} \qquad \text{(S2)}$$

$$\text{AVO–β-CD} \rightarrow \text{AVO} + \text{β-CD} \qquad \text{(S3)}$$

Photostability studies

The effect of complex formation on the photostability of AVO–CB[7] and AVO–β-CD was investigated using UV-Vis spectroscopy, the high-performance liquid chromatography-ultraviolet (HPLC-UV) method, and electrospray ionization mass spectrometry (ESI-MS).

For UV-Vis spectroscopy and HPLC-UV measurements, stock solutions of AVO in ethanol, β-CD in water (15 mM), and CB[7] in water (4 mM) were mixed in quartz tubes (cuvet.co) to prepare 10 mL hydro-alcoholic solutions. The AVO concentration was maintained at 0.006 mM. To explore the influence of host concentration and solvent effects on the photostability of the AVO complexes, solutions were prepared at various guest/host molar ratios (1:5 and 1:10 for AVO–CB[7]; 1:50 and 1:100 for AVO–β-CD) with two different ethanol concentrations (10% and 30%, v/v). Control samples of AVO alone in 10% and 30% ethanol were also prepared. All solutions were exposed to a UV solar simulator for 60 min under magnetic stirring. The UV light source consisted of FS20T12/UVB lamps with a plastic blocking filter to eliminate UVC radiation, resulting in a UVB intensity of 0.24 ± 0.01 mW/cm^2 and a UVA intensity of 5.4 ± 0.1 mW/cm^2 (measured using a UVB and UVA meter from National Biological Corporation). The UVB and UVA doses corresponded to 864 ± 36 mJ/cm^2 and 19440 ± 360 mJ/cm^2, respectively. All experiments were conducted in triplicate. The absorbance spectra of AVO and the AVO complexes were measured before and after irradiation. Degradation, expressed as %recovery, was assessed by comparing the HPLC peak areas of the samples before and after irradiation.

For statistical analysis, the %recovery values were expressed as mean ± SD (standard deviation). Differences were tested using a one-way ANOVA test, and significant differences between groups were identified using Tukey’s HSD post-hoc test. A P-value of <0.05 was considered statistically significant.

For ESI-MS measurements, stock solutions of AVO in ethanol and β-CD or CB[7] in water were mixed in quartz tubes to prepare 12 mL hydro-alcoholic solutions. The AVO concentration was maintained at 0.05 mM, and the guest–host molar ratio was set at 1:1 for both AVO–CB[7] and AVO–β-CD complexes. The ethanol concentration was 10% for AVO–CB[7] and 30% for AVO–β-CD. At irradiation times of 0, 30, and 60 min, 4 mL aliquots were withdrawn and freeze-dried before undergoing ESI-MS analysis.

Results and Discussion

Synthesis of CB[7]

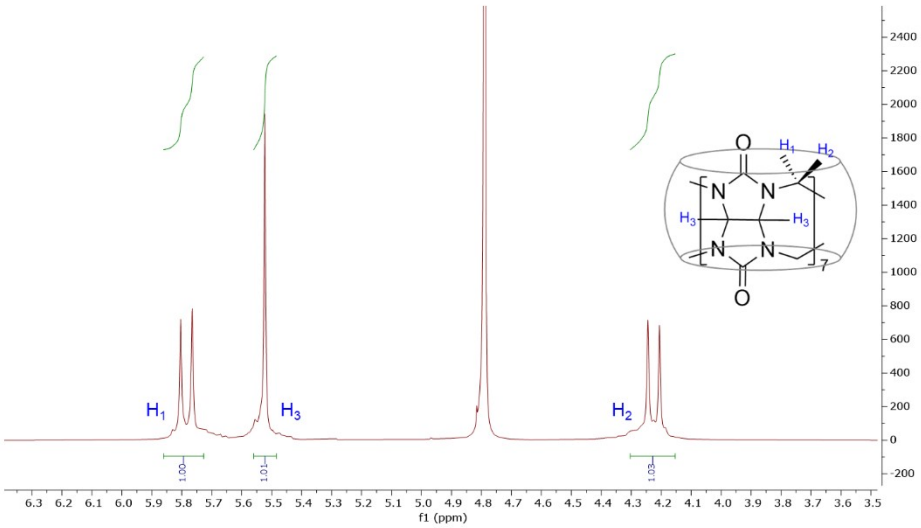

Figure S1. Partial ^{1}H-NMR spectra of CB[7] in D_2O.

Spectroscopy Studies

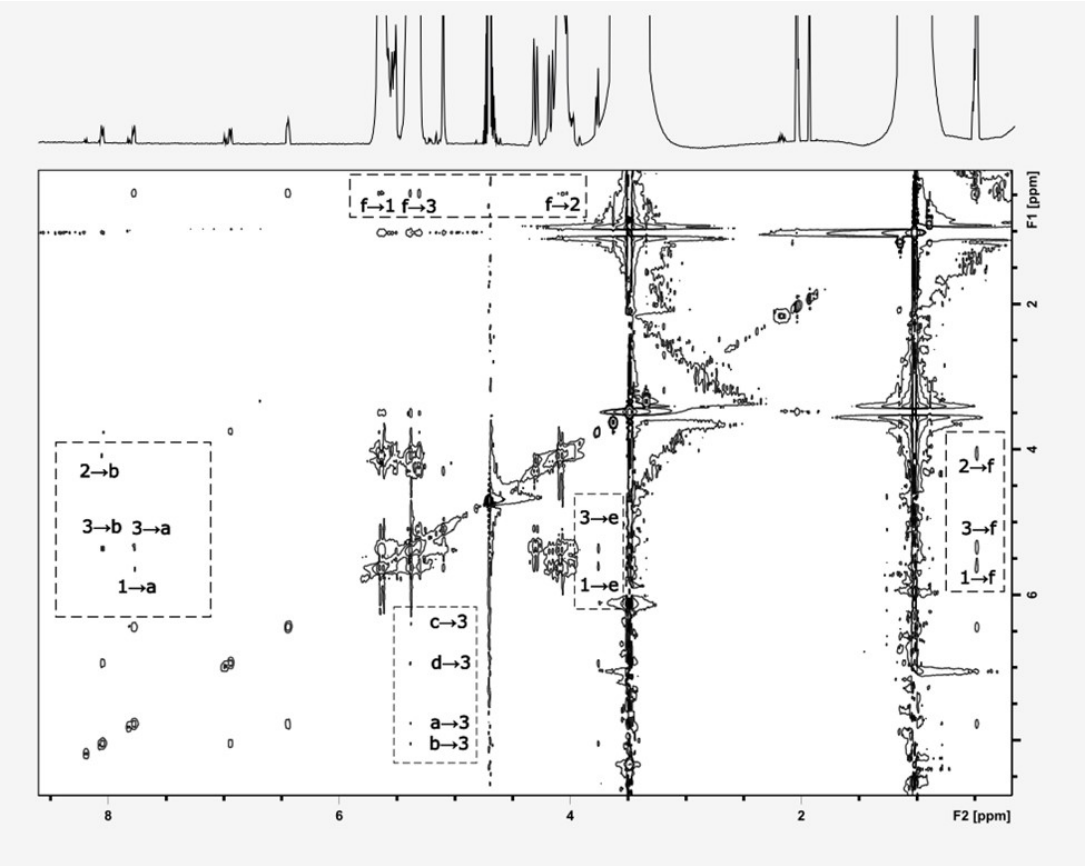

[1]H-NMR

Figure S2. ^{1}H-^{1}H NOESY NMR spectrum of 1:6 AVO:CB[7] in 90% D_2O/10% ethanol-d_1. Boxes surround cross-peaks between AVO and CB[7] resonances.

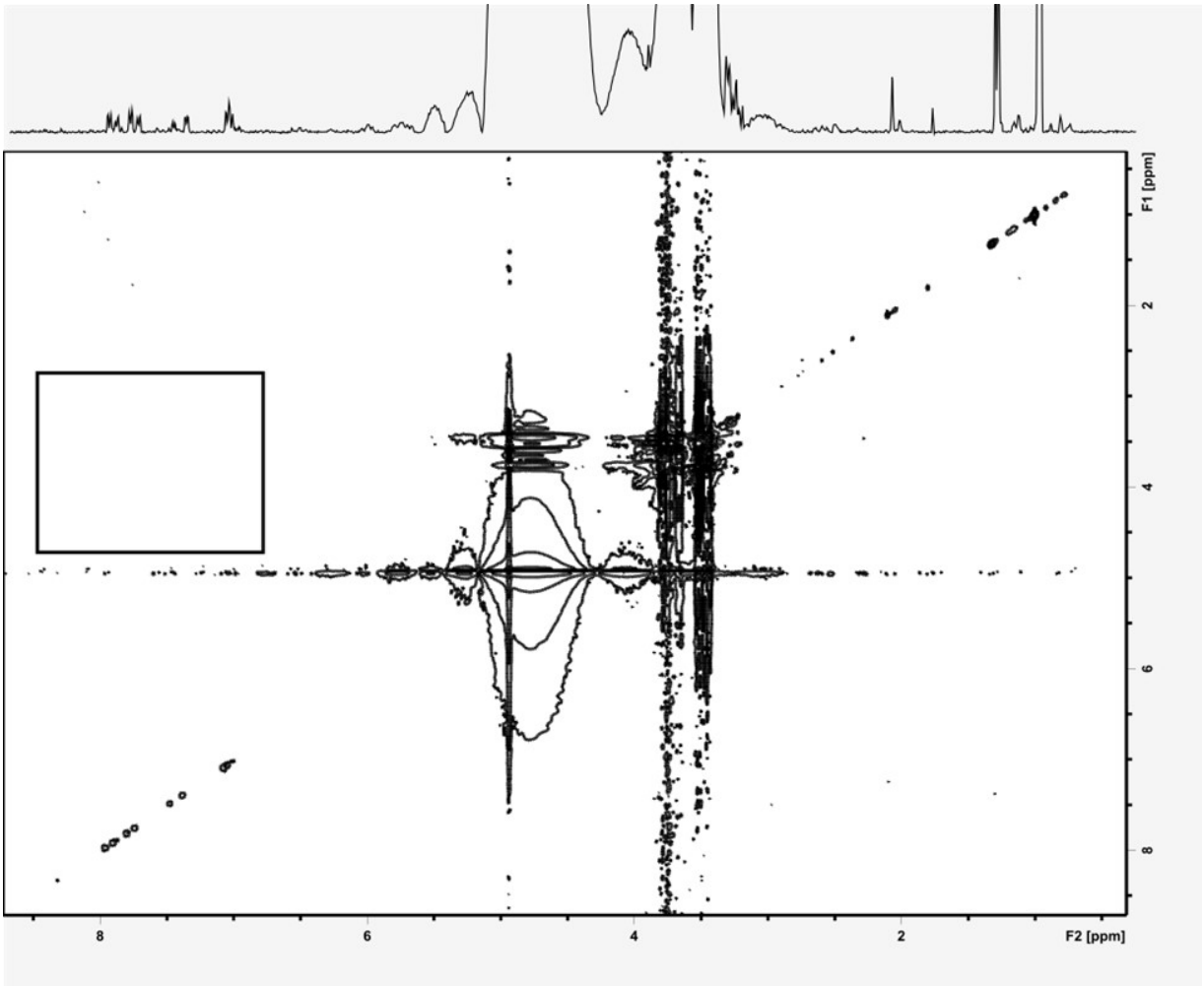

Figure S3. ^{1}H-^{1}H NOESY NMR spectrum of 5:8 AVO:β-CD in 90% D_2O/10% ethanol-d_6. The box is drawn to indicate the location where cross-peaks between the aromatic AVO signals and the β-CD signals would be located.

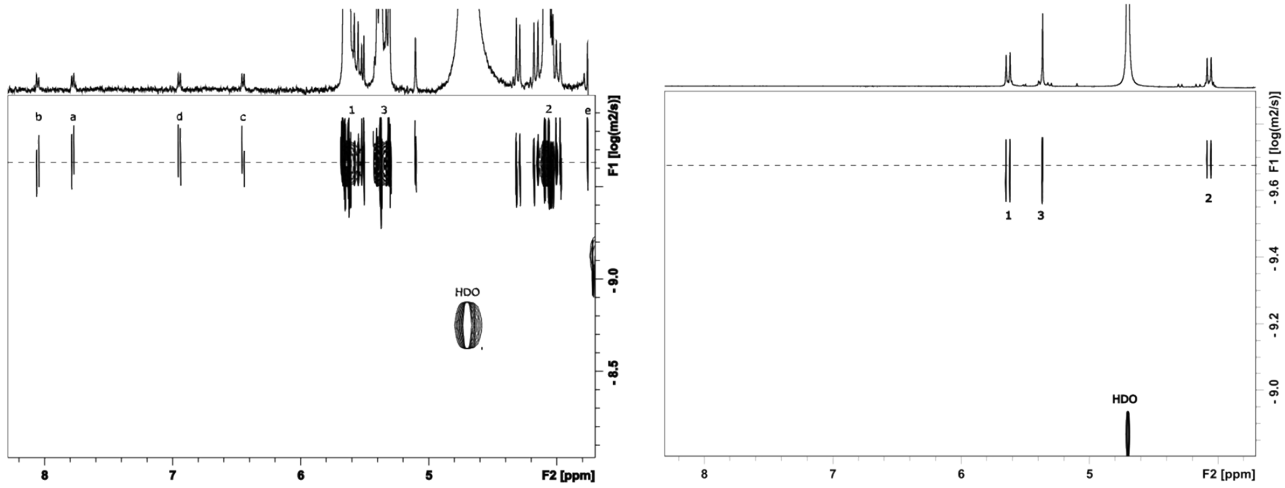

Figure S4. DOSY NMR spectrum of 1:1 AVO:CB[7] in 90% D_2O/10% ethanol-d_1. The dashed horizontal line passes through the AVO aromatic peaks **a-d** and **e** as well as the CB[7] peaks 1-3, indicating very similar diffusion rates for the two compounds (Left). DOSY NMR spectrum of 0.5 mM CB[7] in 90% D_2O/10% ethanol-d_1 (Right).

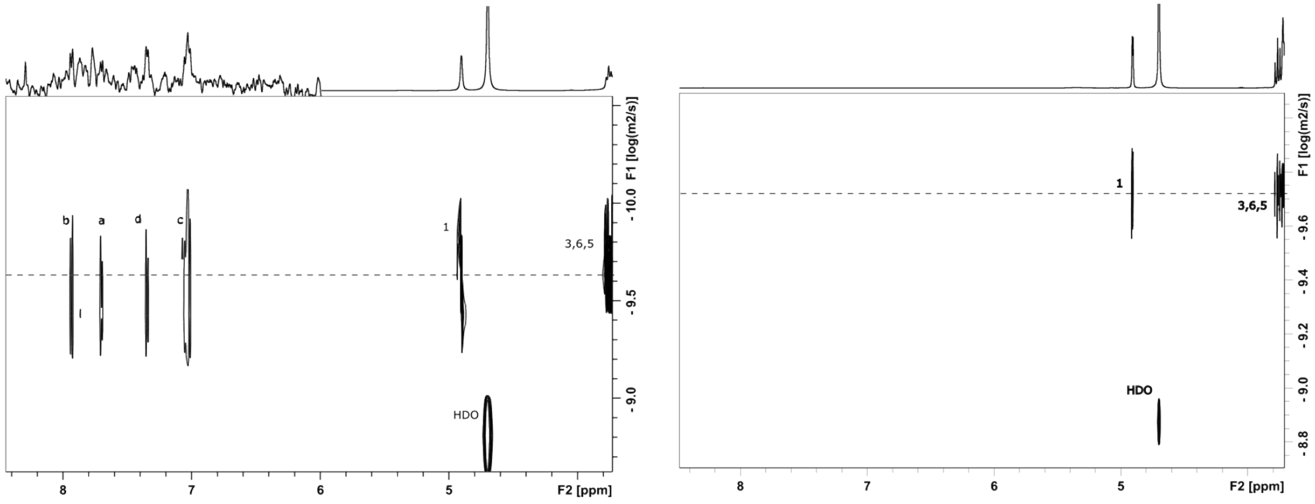

Figure S5. DOSY NMR spectrum of 1:10 AVO:β-CD in 90% D_2O/10% ethanol-d_1. The dashed horizontal line passes through the AVO aromatic peaks **a-d** as well as the β-CD peaks 1, 3, 5, and 6, indicating similar diffusion rates for the two compounds. The vertical scaling is shifted near 6 ppm so that AVO and β-CD peaks are all shown clearly despite the differences in their intensities (Left). DOSY NMR spectrum of 5 mM β-CD in 90% D_2O/10% ethanol-d_1 (Right).

UV-Vis spectroscopy

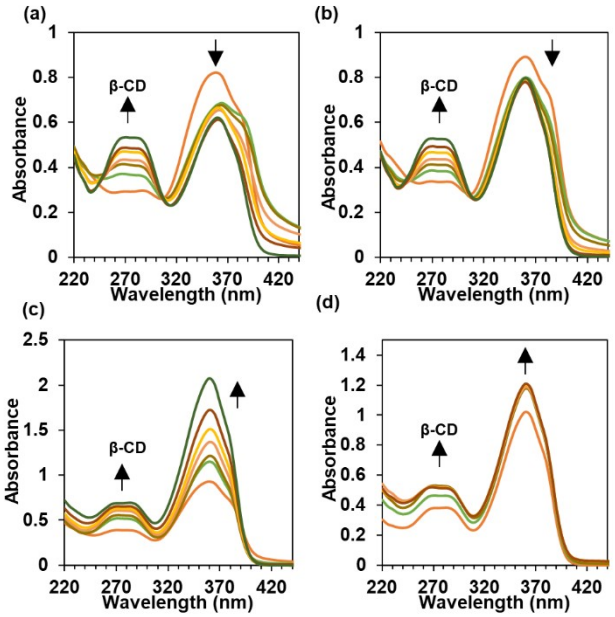

Figure S6. UV-Vis titration spectra for generating the Benesi-Hildebrand plots of AVO (0.04 mM) in the presence of β-CD (0-4 mM) in (a) 10%, (b) 20%, (c) 30% ethanol, and (d) in the presence of β-CD (0-7.5 mM) in 40% ethanol. The absorbance of AVO in 40% ethanol was not significantly higher than that in 30% ethanol due to ethanol's competitive binding to β-CD, which resulted in fewer complexes being formed and consequently reduced absorbance. This agrees with the lower

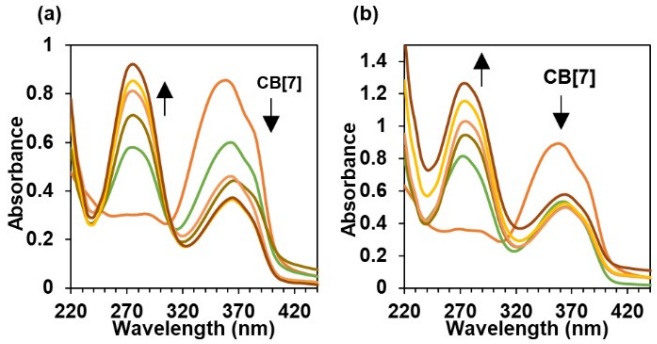

K_a values and molecular dynamics results.

Figure S7. UV-Vis titration spectra for generating the Benesi-Hildebrand plots of AVO (0.04 mM) in the presence of CB[7] (0-2 mM) in (a) 10% and (b) 20% ethanol. UV-Vis titration spectra of AVO in the presence of CB[7] in 30% and 40% ethanol could not be accurately obtained due to the low solubility of CB[7], which caused turbidity.

Benesi-Hildebrand method for determination of stoichiometry and association constant (K_a)

The Benesi-Hildebrand method is a mathematical approach used in the determination of the association constant (K_a) and stoichiometry ratio of non-bonding interaction.

For a 1:1 host (H)-guest (G) complexes,

$$H + G \rightleftharpoons HG$$

$$K_a = \frac{[HG]}{[H][G]}$$

$$K_a = \frac{[HG]}{([H]_0 - [HG])([G]_0 - [HG])}$$

where $[H]_0$ and $[G]_0$ are the initial concentration of host and guest, respectively, $[HG]$ is the concentration of host-guest complex.

The underlining theory of this method is the assumption that when either host or guest is present in excess amount over the other. Then, the absorbance from the small one can be negligible. In this case, the $[G]_0$ or the concentration of AVO is much smaller than host ($[H]_0$). Therefore,

$$K_a = \frac{[HG]}{([H]_0)([G]_0 - [HG])}$$

and $$\Delta A = \Delta\varepsilon b[HG] = \Delta\varepsilon[HG]$$

when $b = 1\ cm$ and $\Delta\varepsilon = \varepsilon^{HG} - \varepsilon^{G}$

by substituting $\Delta A = \Delta\varepsilon[HG]$, $$K_a = \frac{\Delta A/\Delta\varepsilon}{([H]_0)([G]_0 - \Delta A/\Delta\varepsilon)}$$

$$K_a[H]_0 = \frac{\Delta A}{\Delta\varepsilon([G]_0 - \Delta A/\Delta\varepsilon)}$$

$$K_a[H]_0 = \frac{\Delta A}{\Delta\varepsilon[G]_0 - \Delta A}$$

$$K_a[H]_0(\Delta\varepsilon[G]_0 - \Delta A) = \Delta A$$

$$K_a[H]_0\Delta\varepsilon[G]_0 - K_a[H]_0\Delta A = \Delta A$$

$$K_a[H]_0\Delta\varepsilon[G]_0 = \Delta A + K_a[H]_0\Delta A$$

$$K_a[H]_0\Delta\varepsilon[G]_0 = \Delta A(1 + K_a[H]_0)$$

$$\frac{1}{\Delta A} = \frac{1 + K_a[H]_0}{K_a\Delta\varepsilon[H]_0[G]_0}$$

$$\frac{[G]_0}{\Delta A} = \frac{1}{K_a\Delta\varepsilon[H]_0} + \frac{1}{\Delta\varepsilon}$$

where $\Delta A = A - A_0$ is obtained from experiment, with A_0 being the initial absorbance before the interaction and A being the absorbance taken at any point of the reaction.

A plot of $\frac{[G]_0}{\Delta A}$ against $\frac{1}{[H]_0}$ should give a straight line with the slope $= \frac{1}{K_a\Delta\varepsilon}$ and the intercept $= \frac{1}{\Delta\varepsilon}$.

The association constant (K_a) $= \frac{Intercept}{Slope}$ (unit M^{-1})

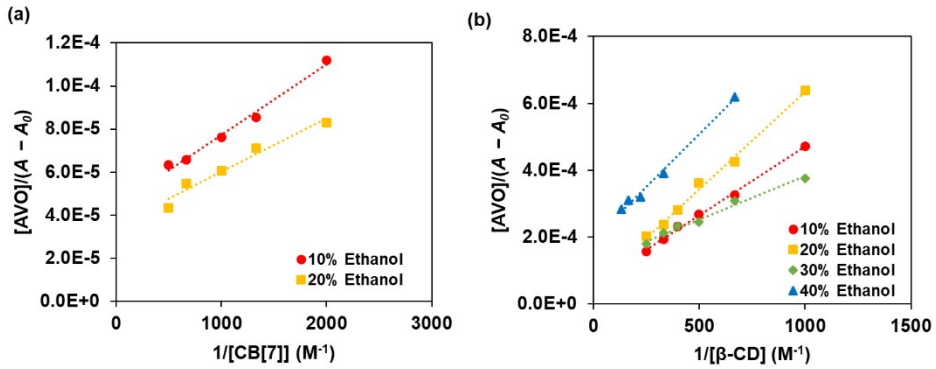

Figure S8. Benesi-Hildebrand plots of (a) 1/[CB[7]] vs [AVO]/(A - A_0) and (b) of 1/[β-CD] vs [AVO]/(A - A_0) from UV-Vis titration data for 1:1 host-guest complex model.

For a 1:2 complexes,

$$2H + G \rightleftharpoons HG$$

$$\frac{[G]_0}{\Delta A} = \frac{1}{K_a \Delta\varepsilon [H]_0^2} + \frac{1}{\Delta\varepsilon}$$

A plot of $\frac{[G]_0}{\Delta A}$ against $\frac{1}{[H]_0^2}$ should give a straight line.

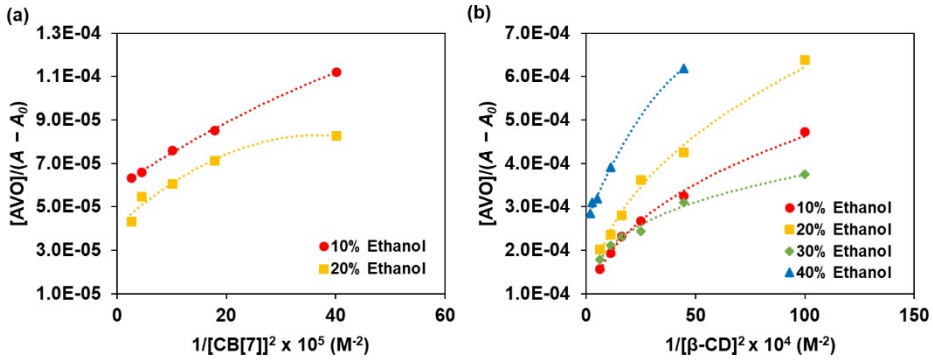

Figure S9. Benesi-Hildebrand plots of (a) 1/[CB[7]]^2 vs [AVO]/(A - A_0) and (b) of 1/[β-CD]^2 vs [AVO]/(A - A_0) from UV-Vis titration data for 1:2 guest-host complex model.

The standard deviation (SD) of K_a can be expressed[13] as $K_a \times \sqrt{\left(\frac{standard\ error\ of\ slope}{slope}\right)^2 + \left(\frac{standard\ error\ of\ intercept}{intercept}\right)^2}$

Table S1. K_a values obtained from the Benesi-Hildebrand method for 1:1 host-guest complexes.

Complexes	% Ethanol	Intercept	Slope	Standard error of intercept	Standard error of slope	R^2	K_a (M^{-1})	*SD*
AVO–β-CD	10	5.73E-05	4.14E-07	6.57E-06	1.13E-08	0.9970	139	16
	20	5.14E-05	5.83E-07	1.25E-05	2.15E-08	0.9946	88	22
	30	1.22E-04	2.60E-07	9.44E-06	1.62E-08	0.9847	468	47
	40	1.93E-04	6.29E-07	1.15E-05	3.19E-08	0.9924	307	24
AVO–CB[7]	10	4.45E-05	3.27E-08	2.59E-06	2.12E-09	0.9876	1358	118
	20	3.51E-05	2.49E-08	3.06E-09	3.74E-06	0.9566	1410	229

Computational studies

Classical MD and electronic structure calculations were used to explore possible interactions between AVO and β-CD or CB[7] in the presence of water or water/ethanol as a solvent. To track these interactions, the radii of the β-CD and CB[7] hosts, the distance between the host center of mass (COM) and the central carbon of *t*-Bu ($C_{t\text{-Bu}}$), the distance between the host COM and the MeO carbon (C_{MeO}), and the distance between $C_{t\text{-Bu}}$ and C_{MeO} were recorded for production runs and all other NPT trajectories (Tables S2–S4). The host radii for β-CD were obtained by determining the COM of the molecule using the heavy atoms in the glucose-based subunits and then measuring the distance to the COM of individual glucose-based subunits; the same process was used for the heavy atoms in the glycouril subunits of CB[7]. The $host_{COM}$–AVO_{COM} values were determined using the COM of all the atoms in the complexes.

Several distances were used as metrics to better understand the simulation results. For all the NPT simulations, regardless of the solvent mixture, the average host radii varied by less than 0.02 Å, demonstrating the robust framework of the hosts, and the β-CD radii was ~ 1 Å greater than that of CB[7] (Tables S2–S4). The distance measured from $host_{COM}$ to $C_{t\text{-Bu}}$ and C_{MeO} varied among the systems depending on the freedom of the AVO molecule. Notably, the systems with an entrapped AVO molecule (e.g., the AVO–CB[7] complex with *t*-Bu within the CB[7] cavity) exhibited much less fluctuation in the $host_{COM}$– $C_{t\text{-Bu}}$ distance compared with the $host_{COM}$–C_{MeO} distance. When entrapped, AVO tended to remain elongated, as evidenced by the longer C_{MeO}– $C_{t\text{-Bu}}$ distances; however, when AVO was not within a host, fewer torsional restrictions resulted in smaller $C_{t\text{-Bu}}$ –C_{MeO} distanceos.

Table S2. Geometric properties of selected AVO–β-CD and AVO–CB[7] complexes.

System/ *Orientation/* Solvent	Distance (Å)				
	host radii	$host_{COM}$–C_{MeO}	$host_{COM}$–C_{tBu}	C_{tBu}–C_{MeO}	$host_{COM}$–AVO_{COM}
AVO–CB[7]					
tBu in CB[7]					
10% EtOH	4.678 ± 0.634	12.540 ± 1.298	0.368 ± 0.159	12.508 ± 1.275	5.720 ± 0.435
20% EtOH	4.678 ± 0.634	12.368 ± 1.335	0.369 ± 0.159	12.322 ± 1.321	5.681 ± 0.450
30% EtOH	4.678 ± 0.632	12.680 ± 1.084	0.362 ± 0.158	12.622 ± 1.086	5.807 ± 0.398
40% EtOH	4.679 ± 0.633	12.534 ± 1.184	0.367 ± 0.159	12.511 ± 1.151	5.721 ± 0.433
MeO in CB[7]					
10% EtOH	4.680 ± 0.649	10.536 ± 0.794	2.897 ± 0.418	12.620 ± 0.816	5.254 ± 0.573
20% EtOH	4.680 ± 0.644	10.466 ± 0.739	2.632 ± 0.400	12.597 ± 0.780	5.183 ± 0.519
30% EtOH	4.679 ± 0.645	10.619 ± 0.785	2.572 ± 0.400	12.673 ± 0.799	5.299 ± 0.562
40% EtOH	4.680 ± 0.647	10.606 ± 0.727	2.615 ± 0.390	12.728 ± 0.781	5.258 ± 0.518
above CB[7] cavity					
10% EtOH	4.666 ± 0.630	23.680 ± 4.591	23.345 ± 5.138	9.398 ± 2.413	23.815 ± 4.730
20% EtOH	4.677 ± 0.661	23.420 ± 5.055	24.872 ± 4.822	9.890 ± 2.474	24.843 ± 4.922
30% EtOH	4.673 ± 0.648	20.058 ± 7.038	19.710 ± 6.543	10.590 ± 1.980	18.968 ± 7.052
40% EtOH	4.675 ± 0.656	24.682 ± 5.590	24.969 ± 6.597	10.296 ± 2.235	24.864 ± 6.548
AVO–β-CD					
tBu in narrow rim					
10% EtOH	5.739 ± 0.204	10.201 ± 1.538	0.917 ± 0.483	10.788 ± 1.627	4.302 ± 0.716
20% EtOH	5.737 ± 0.201	10.793 ± 1.493	0.813 ± 0.440	11.284 ± 1.562	4.594 ± 0.701
30% EtOH	5.742 ± 0.198	10.648 ± 1.567	0.839 ± 0.517	11.052 ± 1.626	4.625 ± 0.785
40% EtOH	5.744 ± 0.195	11.082 ± 1.635	0.792 ± 0.452	11.553 ± 1.680	4.712 ± 0.730
MeO in narrow rim					
10% EtOH	5.752 ± 0.184	7.973 ± 3.216	4.118 ± 3.809	11.277 ± 2.269	3.968 ± 1.415
20% EtOH	5.742 ± 0.223	4.658 ± 2.168	8.464 ± 2.127	12.235 ± 1.549	3.590 ± 1.533
30% EtOH	5.749 ± 0.193	4.971 ± 3.790	7.378 ± 3.156	11.428 ± 2.227	3.806 ± 1.512
40% EtOH	5.741 ± 0.214	9.972 ± 7.976	13.387 ± 6.412	11.404 ± 2.088	10.151 ± 8.692
above narrow rim					
10% EtOH	5.751 ± 0.192	12.946 ± 5.772	5.778 ± 8.533	9.985 ± 2.006	8.776 ± 7.453
20% EtOH	5.737 ± 0.230	23.216 ± 5.067	24.672 ± 4.250	10.230 ± 2.082	24.272 ± 4.696
30% EtOH	5.735 ± 0.232	18.511 ± 5.953	17.295 ± 7.968	10.463 ± 2.277	17.373 ± 7.603
40% EtOH	5.734 ± 0.234	25.247 ± 4.394	24.697 ± 4.399	10.329 ± 2.147	25.003 ± 3.863

Table S3. Geometric properties of AVO-CB(7) and AVO-βCD of initial NPT runs in H_2O.

System/ *Orientation*	Distance Å[a]				
	host radii	$host_{COM}$-C_{MeO}	$host_{COM}$-C_{tBu}	C_{tBu}-C_{MeO}	$host_{COM}$-AVO_{COM}
AVO–CB[7]					
tBu in CB[7]	4.676 ± 0.634	13.256 ± 0.702	0.375 ± 0.163	13.177 ± 0.714	5.919 ± 0.296
	(4.676 ± 0.645)	(13.097 ± 0.804)	(0.371 ± 0.163)	(13.043 ± 0.787)	(5.949 ± 0.295)
MeO in CB[7]	4.681 ± 0.670	2.695 ± 0.361	10.340 ± 0.622	12.632 ± 0.762	5.071 ± 0.424
	(4.679 ± 0.660)	(2.683 ± 0.357)	(10.598 ± 0.669)	(12.832 ± 0.637)	(5.208 ± 0.496)
above CB[7]cavity	4.671 ± 0.634	14.046 ± 3.270	12.320 ± 2.153	7.431 ± 2.391	11.751 ± 1.954
	(4.673 ± 0.632)	(20.849 ± 4.513)	(16.711 ± 4.533)	(9.563 ± 2.884)	(18.304 ± 4.805)
AVO–β-CD					
tBu in wide-rim of β-CD	5.755 ± 0.180	9.611 ± 2.206	1.431 ± 0.993	10.346 ± 1.669	3.834 ± 1.650
	(5.742 ± 0.167)	(13.144 ± 1.051)	(0.744 ± 0.400)	(12.922 ± 0.980)	(6.035 ± 0.540)
above narrow-rim of β-CD	5.711 ± 0.305	18.988 ± 5.932	16.629 ± 5.840	9.861 ± 2.263	16.691 ± 5.289
	(5.723 ± 0.276)	(17.964 ± 4.973)	(25.020 ± 2.565)	(10.118 ± 2.574)	(20.917 ± 2.738)
side of β-CD	5.757 ± 0.205	15.793 ± 1.733	10.190 ± 0.665	9.081 ± 1.751	11.268 ± 0.470
	(5.743 ± 0.230)	(10.990 ± 1.696)	(14.312 ± 3.026)	(9.030 ± 2.113)	(12.287 ± 1.577)
tBu in narrow-rim of β-CD	5.745 ± 0.201	9.452 ± 1.444	0.904 ± 0.453	10.086 ± 1.603	3.937 ± 0.552
	(5.728 ± 0.219)	(9.983 ± 1.169)	(1.080 ± 0.458)	(10.763 ± 1.215)	(4.011 ± 0.553)
MeO in narrow-rim of β-CD	5.762 ± 0.172	7.424 ± 0.816	1.987 ± 1.085	8.681 ± 1.609	2.678 ± 1.073
	(5.745 ± 0.208)	(4.425 ± 1.132)	(8.407 ± 0.707)	(11.387 ± 0.766)	(3.358 ± 0.823)
above wide-rim of β-CD	5.738 ± 0.255	23.489 ±6.078	25.129 ± 3.949	8.822 ± 2.009	24.379 ± 4.136
	(5.751 ± 0.225)	(16.156 ± 2.513)	(15.375 ± 2.655)	(11.191 ± 1.972)	(14.020 ± 1.644)
MeO in wide-rim of β-CD	5.741 ± 0.228	3.296 ± 0.799	6.984 ± 0.596	9.354 ± 1.285	2.991 ± 0.327
	(5.734 ± 0.242)	(2.729 ± 1.000)	(6.487 ± 0.669)	(7.996) ± 1.539)	(3.457 ± 0.954)

[a] Data for 10 Å and 15 Å (in parentheses) truncated octahedron solvent shells.

Table S4. Geometric properties of AVO-CB[7] and AVO-βCD initial NPT runs in 10%, 20%, 30%, and 40% ethanol.

System/ *Orientation/* Solvent	Distance (Å)				
	host radii	$host_{COM}$-C_{MeO}	$host_{COM}$-C_{tBu}	C_{tBu}-C_{MeO}	$host_{COM}$-AVO_{COM}
AVO–CB[7]					
tBu in CB[7]					
10% EtOH	4.676 ± 0.612	13.415 ± 0.594	0.362 ± 0.154	13.375 ± 0.583	5.971 ± 0.261
20% EtOH	4.679 ± 0.644	13.182 ± 0.840	0.361 ± 0.157	13.147 ± 0.862	5.960 ± 0.281
30% EtOH	4.679 ± 0.635	11.896 ± 1.137	0.380 ± 0.167	11.975 ± 1.077	5.510 ± 0.472
40% EtOH	4.684 ± 0.636	12.649 ± 0.969	0.372 ± 0.165	12.573 ± 0.967	5.883 ± 0.316
MeO in CB[7]					
10% EtOH	4.674 ± 0.602	2.648 ± 0.397	10.116 ± 0.557	12.207 ± 0.806	5.014 ± 0.414
20% EtOH	4.680 ± 0.650	2.623 ± 0.403	10.144 ± 0.488	12.241 ± 0.636	5.047 ± 0.415
30% EtOH	4.681 ± 0.654	2.339 ± 0.351	11.279 ± 0.806	13.006 ± 0.767	5.776 ± 0.574
40% EtOH	4.682 ± 0.650	2.602 ± 0.361	10.315 ± 0.678	12.356 ± 0.832	5.137 ± 0.444
above CB[7] cavity					
10% EtOH	4.664 ± 0.629	18.137 ± 3.407	15.510 ± 2.932	10.025 ± 1.423	15.861 ± 1.077
20% EtOH	4.671 ± 0.631	14.463 ± 1.050	10.214 ± 0.424	10.689 ± 1.956	10.291 ± 0.483
30% EtOH	4.675 ± 0.645	18.548 ± 2.834	13.399 ± 3.058	12.152 ± 1.559	14.188 ± 2.265
40% EtOH	4.674 ± 0.635	18.507 ± 2.161	11.626 ± 1.585	10.635 ± 1.468	14.002 ± 1.387
AVO–β-CD					
above narrow-rim of β-CD					
10% EtOH	5.742 ± 0.229	23.868 ± 3.831	18.992 ± 6.008	9.644 ± 2.225	20.859 ± 4.592
20% EtOH	5.733 ± 0.239	15.886 ± 3.111	19.483 ± 2.319	9.861 ± 2.379	17.081 ± 1.695
30% EtOH	5.739 ± 0.220	12.306 ± 3.284	19.119 ± 2.017	11.061 ± 2.288	15.721 ± 1.511
40% EtOH	5.745 ± 0.208	22.461 ± 3.811	26.486 ± 2.447	10.572 ± 2.150	25.420 ± 3.290
tBu in narrow-rim of β-CD					
10% EtOH	5.739 ± 0.204	10.201 ± 1.538	0.917 ± 0.483	10.788 ± 1.627	4.302 ± 0.716
20% EtOH	5.737 ± 0.201	10.793 ± 1.493	0.813 ± 0.440	11.284 ± 1.562	4.594 ± 0.701
30% EtOH	5.742 ± 0.198	10.648 ± 1.567	0.839 ± 0.517	11.052 ± 1.626	4.625 ± 0.785
40% EtOH	5.744 ± 0.195	11.082 ± 1.635	0.792 ± 0.452	11.553 ± 1.680	4.712 ± 0.730
MeO in narrow-rim of β-CD					
10% EtOH	5.747 ± 0.205	4.607 ± 1.140	8.578 ± 0.908	12.240 ± 0.792	3.289 ± 0.935
20% EtOH	5.740 ± 0.202	4.195 ± 1.631	9.304 ± 1.613	12.152 ± 1.450	4.090 ± 1.826
30% EtOH	5.741 ± 0.233	3.416 ± 1.130	10.088 ± 1.615	12.543 ± 1.089	4.633 ± 1.360
40% EtOH	5.742 ± 0.210	2.446 ± 1.405	9.946 ± 1.160	11.128 ± 0.894	5.434 ± 1.394

Table S5. Geometric data for B3LYP/6-311G(d,p) calculations.

System	Distance (Å)		
orientation	host radii	$host_{COM}$-C_{tBu}	C_{tBu}-C_{MeO}
CB[7]	5.026		
AVO–CB[7]			
tBu in CB[7]	5.028 ± 0.066	11.833	0.544
MeO in CB[7]	5.022 ± 0.218	4.694	8.925
above CB[7] cavity	5.019 ± 0.009	12.943	8.559
β-CD	5.715		
AVO–β-CD			
tBu in wide-rim of β-CD	5.718 ± 0.119	13.207	4.954
above narrow-rim of β-CD	5.708 ± 0.089	12.598	9.670
side of β-CD	5.716 ± 0.128	12.598	9.670
tBu in narrow-rim of β-CD	5.711 ± 0.085	9.933	4.098
MeO in narrow-rim of β-CD	5.725 ± 0.140	1.533	10.593
above wide-rim of β-CD	5.713 ± 0.071	8.339	2.307

Table S6. Relative thermodynamic values of selected AVO–CB[7] and AVO–β-CD complexes.

System/ *Orientation*	Δ*H* (Δ*G*)[a]	Δ*H* (Δ*G*)[a]	Δ*H* (Δ*G*)[a]
	gas phase[b]	H_2O	EtOH
AVO–CB[7]			
tBu in CB[7]	0.0, 0.0 (0.0, 0.0)	0.0, 0.0 (0.0, 0.0)	0.0, 0.0 (0.0, 0.0)
MeO in CB[7]	5.2, 7.5 (-18.1, -5.4)	27.5, 40.2 (9.4, 22.1)	30.2, 42.9 (13.0, 25.7)
above CB[7]	56.9, 44.9 (16.0, 4.0)	91.1, 79.2 (50.5, 38.5)	82.8, 70.8 (41.9, 29.9)
AVO–β-CD			
tBu in narrow rim of β-CD	0.0, 0.0 (0.0, 0.0)	0.0, 0.0 (0.0, 0.0)	0.0, 0.0 (0.0, 0.0)
tBu in wide rim of β-CD	8.9, 20.3 (-13.7, -2.3)	19.0, 30.4 (-4.4, 7.1)	14.3, 25.7 (-8.9, 2.5)
above narrow rim of β-CD	30.0, 31.3 (-0.6, 0.7)	37.4, 38.6 (6.5, 7.8)	28.7, 30.0 (-1.9, -0.6)
MeO in narrow rim of β-CD	35.0, 38.7 (19.3, 22.9)	37.5, 41.1 (23.8, 27.4)	36.2, 39.8 (22.2, 25.9)
side of β-CD	53.0, 52.8 (12.1, 11.9)	80.7, 80.5 (40.2, 40.0)	70.4, 70.2 (29.9, 29.7)
above wide rim of β-CD	666.3, 896.3 (650.9, 880.9)	651.5, 881.5 (636.6, 866.6)	650.3, 880.3 (635.4, 865.4)

[a] All data in kJ/mol for B3LYP/6-311G(d,p) optimized structures. The Δ*H* and Δ*G* values separated by commas correspond to ωB97X-D/6-311+G(d,p) and M06-2X/6-311+G(d,p) SPE calculations.
[b] BSSE corrected values.

Table S7. BDEs and BDFs of AVO-CB[7] and AVO-β-CD[a]

system calculational level	Δ*H* (Δ*G*)[a]	Δ*H* (Δ*G*)[a]	Δ*H* (Δ*G*)[a]
	gas phase[b]	H_2O	C_2H_5OH
AVO–CB[7]			
ωB97X-D/6-311+G(d,p)	121.4 (63.3)	124.6 (66.6)	114.2 (56.1)
ωB97X-D/6-311G(d,p)	118.8 (60.8)	145.5 (87.4)	134.3 (76.3)
M06-2X/6-311+G(d,p)	69.7 (11.6)	74.5 (16.4)	63.6 (5.5)
M06-2X/6-311G(d,p)	66.2 (8.1)	95.4 (37.3)	84.0 (25.9)
AVO–β-CD			
ωB97X-D/6-311+G(d,p)	102.6 (62.8)	100.1 (60.3)	93.5 (53.6)
ωB97X-D/6-311G(d,p)	93.6 (53.8)	108.4 (68.6)	101.3 (61.5)
M06-2X/6-311+G(d,p)	48.6 (8.7)	47.3 (7.5)	40.7 (0.8)
M06-2X/6-311G(d,p)	39.1 (-0.8)	53.3 (13.4)	46.1 (6.3)

[a]All data in kJ/mol. Reactions of most favorable orientation according to equations 2 and 3.
[b]BSSE corrected values.

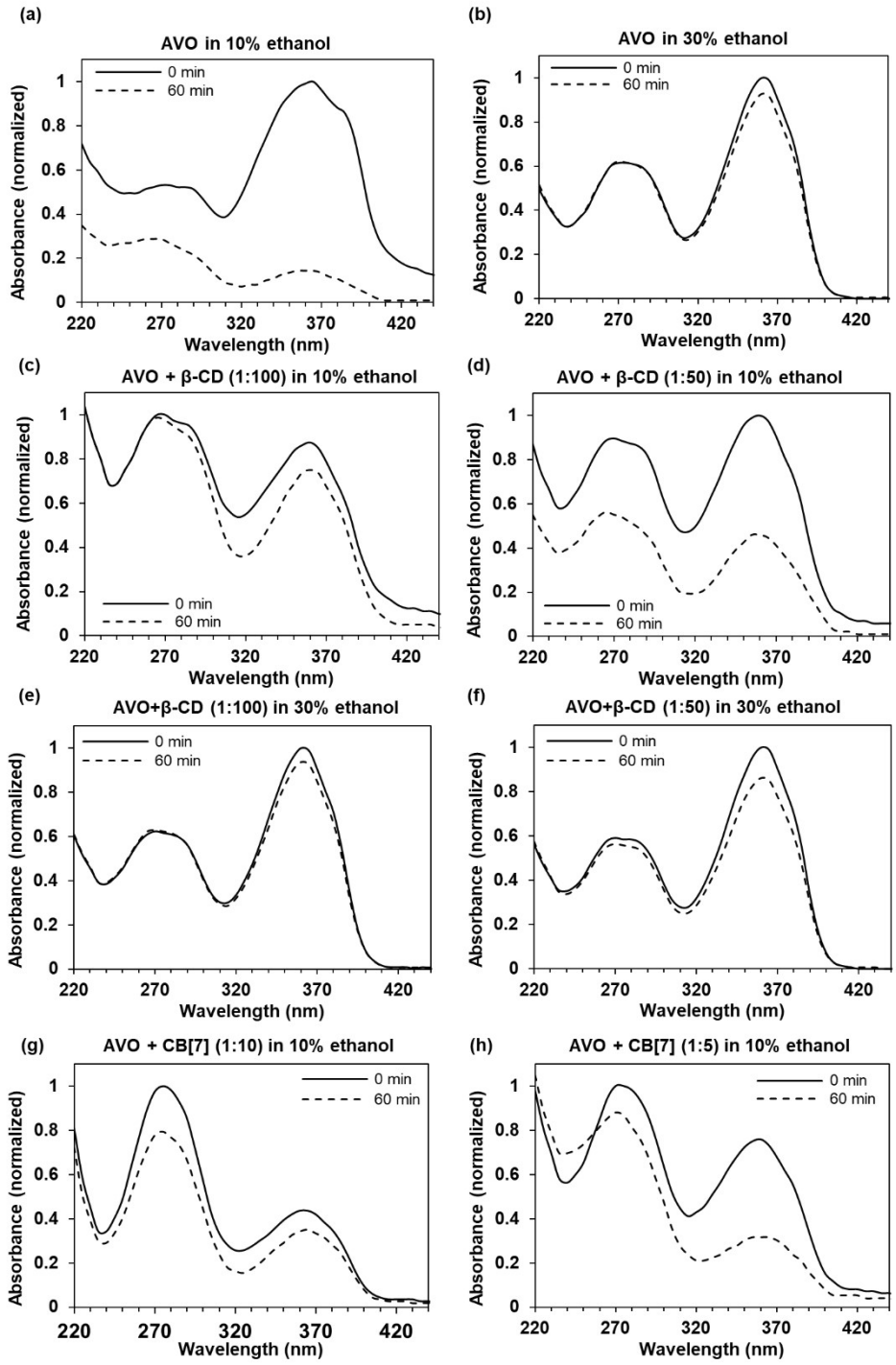

Photostability studies

Figure S10. Changes in the absorption spectrum of AVO in (a) 10% and (b) 30% ethanol/water, AVO–β-CD complexes in 10% ethanol/water at (c) 1:100 and (d) 1:50 molar ratio, AVO–β-CD complexes in 30% ethanol/water at (e) 1:100 and (f) 1:50 molar ratio, and AVO–CB[7] complexes in 10% ethanol/water at (g) 1:10 and (g) 1:5 molar ratio before and after UV exposure (an UVB intensity of 0.24 ± 0.01 mW/cm^2 and an UVA intensity of 5.4 ± 0.1 mW/cm^2; exposure time: 60 min).

Table S8. Effect of β-CD and CB[7] on the photostability of AVO in solutions after 60-min irradiation, expressed as %recovery.

Guest + Host (molar ratio)	%Recovery (mean ± SD)	
	10% ethanol	30% ethanol
AVO	6.2 ± 2.41	88.2 ± 8.73
AVO + β-CD (1:100)	55.7 ± 6.20	93.3 ± 4.74
AVO + β-CD (1:50)	32.7 ± 1.84	95.2 ± 6.72
AVO + CB[7] (1:10)	56.6 ± 4.37	-
AVO + CB[7] (1:5)	20.4 ± 2.14	-

Calculating the concentrations of bound avobenzone in solutions for photostability experiments

For a 1:1 host (H)-guest (G) complexes,

$$H + G \rightleftharpoons HG$$

$$K_a = \frac{[HG]}{[H][G]}$$

$$K_a = \frac{[HG]}{([H]_t - [HG])([G]_t - [HG])}$$

where $[H]_t$ and $[G]_t$ are the total concentration of host and guest, respectively, $[HG]$ is the concentration of host-guest complex, $[H]$ and $[G]$ are the concentration of free host and guest, respectively.

$$K_a[HG]^2 - \{([H]_t + [G]_t)K_a + 1\}[HG] + ([H]_t[G]_t)K_a = 0$$

For a polynomial equation,

$$ax^2 + bx + c = 0$$

$$x = \frac{-b \pm \sqrt{b^2 - 4ac}}{2a}$$

where $[HG] = x$

$K_a = a$

$-\{([H]_t + [G]_t)K_a + 1\} = b$

$([H]_t[G]_t)K_a = c$

and $[HG] \leq [H]_t \; and \; [G]_t$

therefore, $[G] = [G]_t - [HG]$

Table S9. The percentage of bound AVO in ethanol/water (%v/v) solutions for photostability experiments calculated using K_a obtained from the Benesi-Hildebrand method as shown in Table S1.

Complex systems	$[G]_t$ (mM)	$[H]_t$ (mM)	a	b	c	$[HG]$ (mM)	$[H]$	% bound AVO
AVO + βCD (1:100) in 10%	0.006	0.6	139	-85.2	0.500	0.00593	7.18×10^{-5}	98.8
AVO + βCD (1:50) in 10%	0.006	0.3	139	-43.5	0.250	0.00586	1.43×10^{-4}	97.6
AVO + βCD (1:100) in 30%	0.006	0.6	468	-284.6	1.685	0.00598	2.15×10^{-5}	99.6
AVO + βCD (1:50) in 30%	0.006	0.3	468	-144.2	0.842	0.00596	4.33×10^{-5}	99.3
AVO + CB[7] (1:10) in 10%	0.006	0.06	1358	-90.6	0.489	0.00592	8.06×10^{-5}	98.7
AVO + CB[7] (1:5) in 10%	0.006	0.03	1358	-49.9	0.244	0.00582	1.77×10^{-4}	97.0

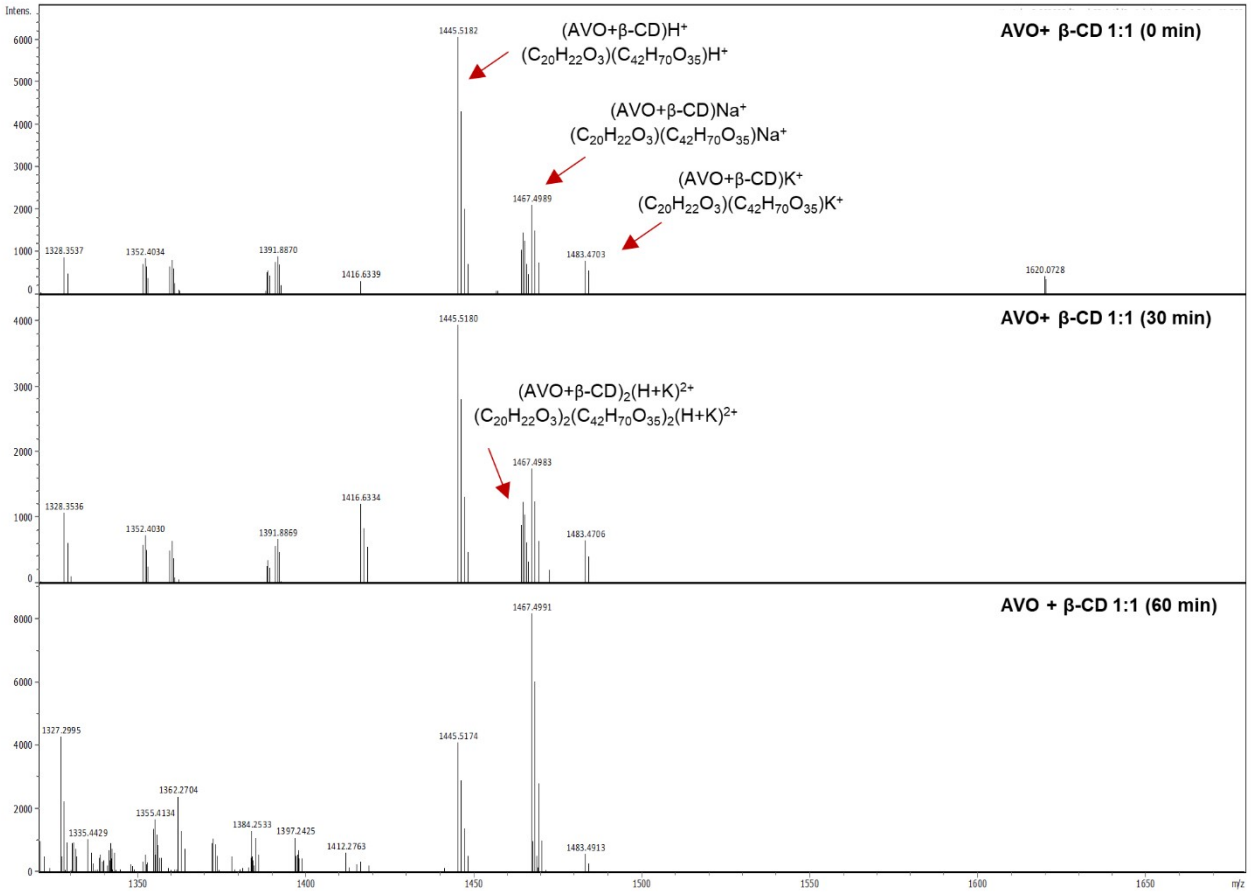

Figure S11. Stacked plot of MS spectra for AVO–β-CD complex (1:1 molar ratio) before (0 min), after 30 and 60 min UV irradiation.

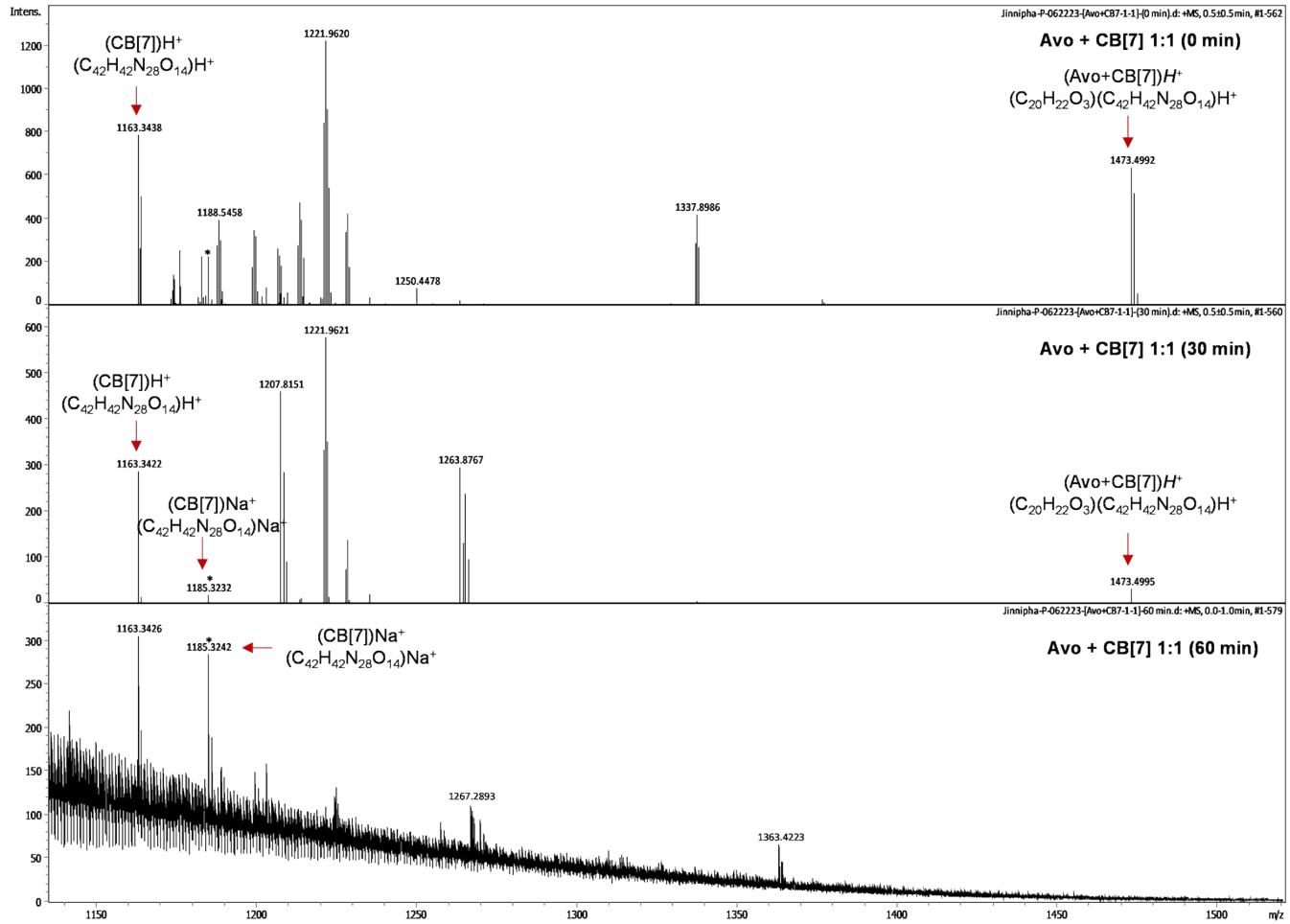

Figure S12. Stacked plot of MS spectra for AVO–CB[7] complex (1:1 molar ratio) before (0 min), after 30 and 60 min UV irradiation.

Table S10. List of the m/z peaks found in the ESI-MS spectra of 60 min irradiatted AVO–βCD and AVO–CB[7].

m/z	Adduct ions	Formula
311.1626	$(AVO)H^+$	$(C_{20}H_{22}O_3)H^+$
333.1433	$(AVO)Na^+$	$(C_{20}H_{22}O_3)Na^+$
643.2965	$(AVO)_2Na^+$	$(C_{20}H_{22}O_3)_2Na^+$
734.2499	$(AVO+β\text{-}CD)(H+Na)^{2+}$	$(C_{20}H_{22}O_3)(C_{42}H_{70}O_{35})(H+Na)^{2+}$
742.2385	$(AVO+β\text{-}CD)(H+K)^{2+}$	$(C_{20}H_{22}O_3)(C_{42}H_{70}O_{35})(H+K)^{2+}$
1135.3657	$(β\text{-}CD)H^+$	$(C_{42}H_{70}O_{35})H^+$
1157.3469	$(β\text{-}CD)Na^+$	$(C_{42}H_{70}O_{35})Na^+$
1163.3426	$(CB[7])H^+$	$(C_{42}H_{42}N_{28}O_{14})H^+$
1185.3219	$(CB[7])Na^+$	$(C_{42}H_{42}N_{28}O_{14})Na^+$
1445.5182	$(AVO+β\text{-}CD)H^+$	$(C_{20}H_{22}O_3)(C_{42}H_{70}O_{35})H^+$
1464.4938	$(AVO+β\text{-}CD)_2(H+K)^{2+}$	$(C_{20}H_{22}O_3)_2(C_{42}H_{70}O_{35})_2(H+K)^{2+}$
1467.4990	$(AVO+β\text{-}CD)Na^+$	$(C_{20}H_{22}O_3)(C_{42}H_{70}O_{35})Na^+$
1473.4992	$(AVO+CB[7])H^+$	$(C_{20}H_{22}O_3)(C_{42}H_{42}N_{28}O_{14})H^+$
1483.4703	$(AVO+β\text{-}CD)K^+$	$(C_{20}H_{22}O_3)(C_{42}H_{70}O_{35})K^+$

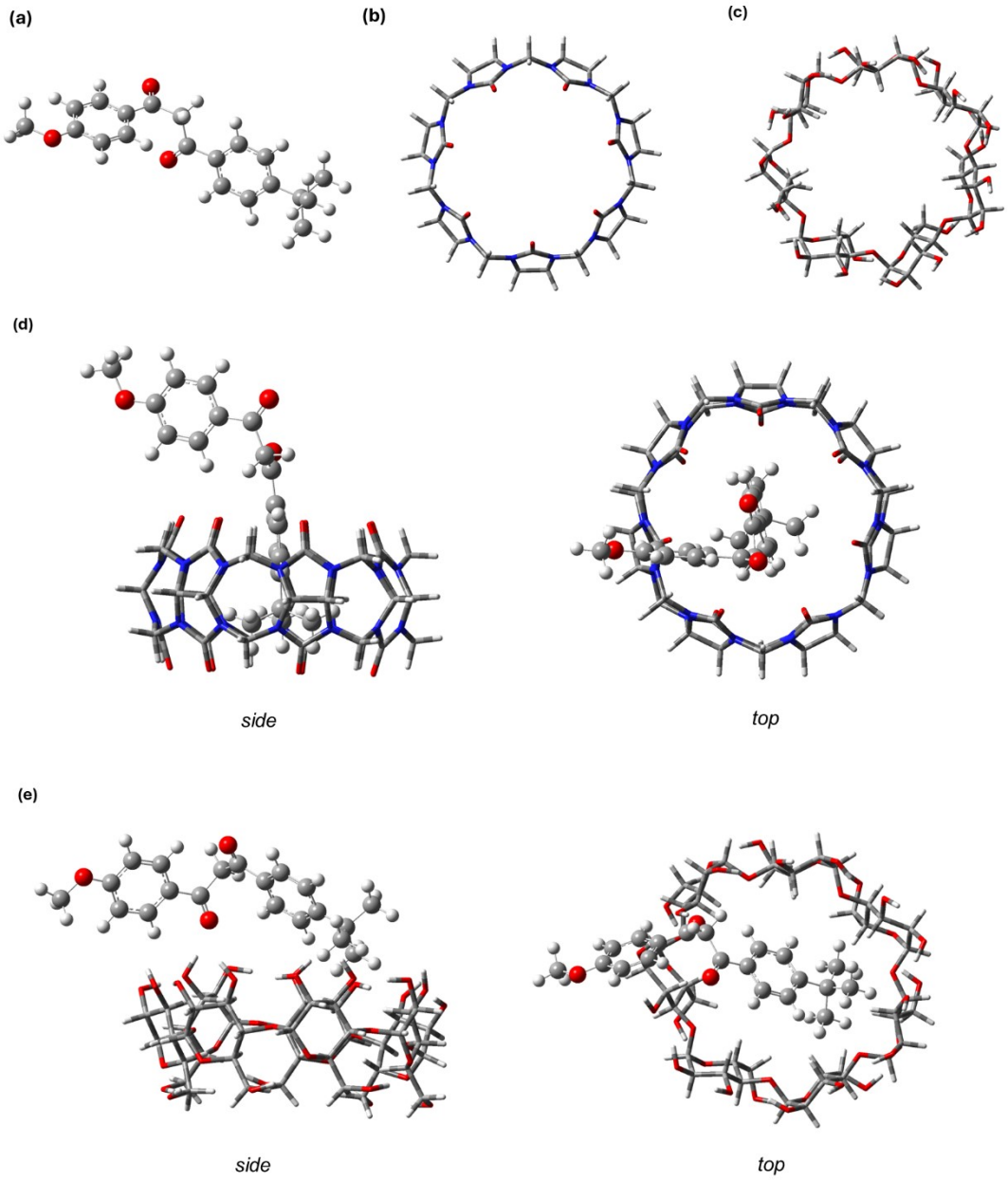

Figure S13. The DFT-optimized structure of (a) AVO, (b) CB[7], (c) β-CD, (d) side and top views of AVO–CB[7] complex, and (e) side and top views of β-CD complex using B3LYP/6-311G(d,p).

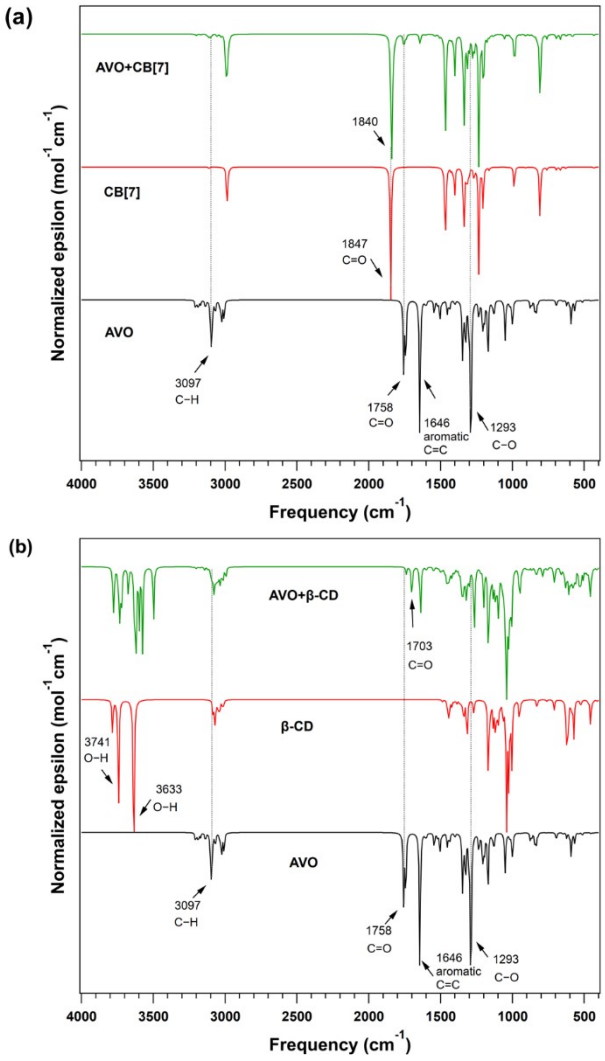

Figure S14. The DFT calculated IR spectra of (a) (top to bottom) AVO–CB[7] complex, CB[7], and AVO; (b) (top to bottom) AVO–β-CD complex, β-CD, and AVO on the gaseous phase using the B3LYP/6-311G(d,p).

References

[1] H. M. A. D.A. Case, K. Belfon, I.Y. Ben-Shalom, J.T. Berryman, S.R. Brozell, D.S. Cerutti, T.E. Cheatham, III, G.A. Cisneros, V.W.D. Cruzeiro, T.A. Darden, N. Forouzesh, G. Giambaşu, T. Giese, M.K. Gilson, H. Gohlke, A.W. Goetz, J. Harris, S. Izadi, S.A. Izmailov, K. Kasavajhala, M.C. Kaymak, E. King, A. Kovalenko, T. Kurtzman, T.S. Lee, P. Li, C. Lin, J. Liu, T. Luchko, R. Luo, M. Machado, V. Man, M. Manathunga, K.M. Merz, Y. Miao, O. Mikhailovskii, G. Monard, H. Nguyen, K.A. O'Hearn, A. Onufriev, F. Pan, S. Pantano, R. Qi, A. Rahnamoun, D.R. Roe, A. Roitberg, C. Sagui, S. Schott-Verdugo, A. Shajan, J. Shen, C.L. Simmerling, N.R. Skrynnikov, J. Smith, J. Swails, R.C. Walker, J. Wang, J. Wang, H. Wei, X. Wu, Y. Wu, Y. Xiong, Y. Xue, D.M. York, S. Zhao, Q. Zhu, and P.A. Kollman, University of California, San Francisco, **2023**.

[2] X. He, V. H. Man, W. Yang, T. S. Lee, J. Wang, *J Chem Phys* **2020**, *153*, 114502.

[3] J. Wang, W. Wang, P. A. Kollman, D. A. Case, *J Mol Graph Model* **2006**, *25*, 247-260.

[4] W. L. Jorgensen, J. Chandrasekhar, J. D. Madura, R. W. Impey, M. L. Klein, *The Journal of Chemical Physics* **1983**, *79*, 926-935.

[5] G. S. Grest, K. Kremer, *Phys Rev A Gen Phys* **1986**, *33*, 3628-3631.

[6] J.-P. Ryckaert, G. Ciccotti, H. J. C. Berendsen, *Journal of Computational Physics* **1977**, *23*, 327-341.

[7] aT. Darden, D. York, L. Pedersen, *The Journal of Chemical Physics* **1993**, *98*, 10089-10092; bU. Essmann, L. Perera, M. L. Berkowitz, T. Darden, H. Lee, L. G. Pedersen, *The Journal of Chemical Physics* **1995**, *103*, 8577-8593.

[8] D. R. Roe, T. E. Cheatham, III, *Journal of Chemical Theory and Computation* **2013**, *9*, 3084-3095.

[9] E. F. Pettersen, T. D. Goddard, C. C. Huang, G. S. Couch, D. M. Greenblatt, E. C. Meng, T. E. Ferrin, *Journal of Computational Chemistry* **2004**, *25*, 1605-1612.

[10] M. J. Frisch, G. W. Trucks, H. B. Schlegel, G. E. Scuseria, M. A. Robb, J. R. Cheeseman, G. Scalmani, V. Barone, G. A. Petersson, H. Nakatsuji, X. Li, M. Caricato, A. V. Marenich, J. Bloino, B. G. Janesko, R. Gomperts, B. Mennucci, H. P. Hratchian, J. V. Ortiz, A. F. Izmaylov, J. L. Sonnenberg, Williams, F. Ding, F. Lipparini, F. Egidi, J. Goings, B. Peng, A. Petrone, T. Henderson, D. Ranasinghe, V. G. Zakrzewski, J. Gao, N. Rega, G. Zheng, W. Liang, M. Hada, M. Ehara, K. Toyota, R. Fukuda, J. Hasegawa, M. Ishida, T. Nakajima, Y. Honda, O. Kitao, H. Nakai, T. Vreven, K. Throssell, J. A. Montgomery Jr., J. E. Peralta, F. Ogliaro, M. J. Bearpark, J. J. Heyd, E. N. Brothers, K. N. Kudin, V. N. Staroverov, T. A. Keith, R. Kobayashi, J. Normand, K. Raghavachari, A. P. Rendell, J. C. Burant, S. S. Iyengar, J. Tomasi, M. Cossi, J. M. Millam, M. Klene, C. Adamo, R. Cammi, J. W. Ochterski, R. L. Martin, K. Morokuma, O. Farkas, J. B. Foresman, D. J. Fox, Wallingford, CT, **2016**.

[11] R. K. Dennington, Todd A.; Millam, John M. , Semichem Inc., Shawnee Mission, KS, **2016**.

[12] M. J. Márquez, M. B. Márquez, P. G. Cataldo, S. A. Brandán, *Open Journal of Synthesis Theory and Applications* **2015**, *04*, 1-19.

[13] G. Chalumot, C. Yao, V. Pino, J. L. Anderson, *JOURNAL OF CHROMATOGRAPHY A* **2009**, *1216*, 5242-5248.